EARTH SURFACE PROCESSES AND LANDFORMS
Earth Surf. Process. Landforms **39**, 1365–1377 (2014)

Published online 20 May 2014 in Wiley Online Library
(wileyonlinelibrary.com) DOI: 10.1002/esp.3588

Modeling planform evolution of a mud-dominated meandering river: Quinn River, Nevada, USA

Yo Matsubara and Alan D. Howard*
Department of Environmental Sciences, University of Virginia, PO Box 400123, Charlottesville, VA 22904-4123, USA

Received 28 August 2012; Revised 4 April 2014; Accepted 7 April 2014

*Correspondence to: A. D. Howard, Department of Environmental Sciences, University of Virginia, PO Box 400123, Charlottesville, VA 22904-4123, USA.
E-mail: ah6p@Virginia.EDU

ESPL
Earth Surface Processes and Landforms

ABSTRACT: A depth-averaged linearized meander evolution model was calibrated and tested using the field data collected at the Quinn River in the Black Rock Desert, Nevada. Two approaches used to test the model were: (1) simulating meander evolution and comparing the results with the observed 38 year migration pattern; and (2) fitting the model parameters to present bank asymmetry (the ratio of the maximum bank gradients on opposite sides of the channel). The data required as input were collected in the field during a high flow in May 2011 and from aerial photographs and LiDAR data. Both approaches yielded similar results for the best fit parameter values. The bank asymmetry analysis showed that the bank asymmetry and the velocity perturbation have high correlation at close to zero spatial lag while the maximum correlation between the bank asymmetry and maximum bend curvature is offset by about 25 m. The model sufficiently replicated 38 years of channel migration, with a few locations significantly under- or over-predicted. Inadequacies of the flow model and/or variation in bank properties unaccounted for are most likely the causes for these discrepancies. Flow through the Quinn River was also simulated by a more general 3D model. The downstream pattern of near-bank shear stresses simulated by the 3D model is nearly identical to those resulting from the linearized flow model. Topographic profiles across interior bends are essentially invariant over a wide range of migration rates, suggesting that the traditional formulation that cut bank erosion processes govern migration rates is appropriate for the Quinn River. Copyright © 2014 John Wiley & Sons, Ltd.

KEYWORDS: meander; river; modeling; mud; bank erosion

Introduction

Meandering channels are of interest to both engineers and geomorphologists. Study of meandering is of intrinsic interest as an evolving quasi-periodic natural system (Seminara, 2006; Seminara and Pittaluga, 2012), and because of the practical issue of predicting meander migration for infrastructure planning and disaster prevention. The difficulty in predicting meander migration over time is due to the interaction of multiple processes all of which have their own time scale yet interact with each other greatly (Ottevanger *et al.*, 2012). One of such processes is the interaction between the river and the banks. Channel meandering is typically associated with a vegetation cover that provides bank strength through cohesion, which depends on the types and state (e.g. age, health, extent of cover) of vegetation, which makes modeling meander evolution more complex (Perucca *et al.*, 2007; Crosato and Saleh, 2011; Güneralp and Rhoads, 2011; Parker *et al.*, 2011).

Many studies have been conducted from both geomorphological (Leopold and Wolman, 1960; Nanson and Hickin, 1983; Engel and Rhoads, 2012) and fluid dynamical approaches (Ikeda *et al.*, 1981; Johannesson and Parker, 1989; Howard, 1992, 1996; Constantine *et al.*, 2009; Güneralp and Rhoads, 2011; Chen and Tang, 2012; Luchi *et al.*, 2012; Motta *et al.*, 2012; Ottevanger *et al.*, 2012) to further the understanding of meander mechanics. Laboratory flume experiments are particularly useful to observe how the flow field interacts with the morphology of the channel in a controlled setting (Blanckaert, 2009, 2010, 2011). Various models are available to study the fluid dynamics of a meandering channel and/or simulate the meander migration pattern with complexities ranging from linearized meander evolution models (Ikeda *et al.*, 1981; Howard and Knutson, 1984; Crosato, 1987; Johannesson and Parker, 1989 Larsen *et al.*, 2006; Camporeale *et al.*, 2007; Güneralp and Rhoads, 2009, 2010) to full 3D fluid dynamic models (Keylock *et al.*, 2005; van Sabben, 2010; Constantinescu *et al.*, 2013) that have no geometric restrictions but are computationally expensive and much more complex (Camporeale *et al.*, 2007). Yet meander mechanics are still not fully understood especially for rivers dominated by the transport of fine sediments.

Since the original 1D meander flow model of Ikeda *et al.* (1981) a number of additional models have been proposed. The Johannesson and Parker (1989) (abbreviated J&P hereafter) model extends the Ikeda *et al.* (1981) model to include the convective transport of flow momentum by the secondary flow. Several subsequent models have addressed the interaction of migrating and curvature-induced bars, including resonances between these bars and the relative importance of upstream and downstream flow influences in meandering (Seminara and Tubino, 1989; Tubino and Seminara, 1990; Seminara *et al.*, 2001; Zolezzi and Seminara, 2001).

The strongly meandering, silt and clay-dominated Quinn river provides an excellent setting for evaluating quantitative models of meander flow and channel migration. The banks at the Quinn River are nearly devoid of vegetation, removing one potential factor contributing to variability in bank erosion rates. A 22.7 km channel reach covered by LiDAR topography contains 30+ full meanders to provide a 40 year record of bend migration. The narrow, nearly constant width channel with steep banks closely approximates the idealized channel cross-section for the linearized J&P flow model. The very low-water LiDAR topography permits comparative 3-D flow modeling using Delft3D. We use a goodness-of-fit criterion between predicted versus observed meander migration to evaluate the performance of the J&P flow model and bend erosion assumptions, including a spatially variable bank erosion factor (relative bank height). The modeling is also used to evaluate the importance of floodplain heterogeneity as an influence on meander migration. The cross-correlation between the downstream variation of the channel cross-sectional asymmetry and near-bank shear stress predicted by the J&P and Delf3D models provides a sensitive test of model performance in predicting bank erosion patterns. Similar cross-correlation is used to evaluate systematic width variations as related to flow and bend curvature. Delf3D flow modeling is used to evaluate the performance of the 1-D J&P model in sharp bends where the linear approximation of the J&P model is likely to be inaccurate.

The purpose of this study is to test the capacity of the J&P model of river meandering to predict planform evolution of a mud-dominated river using field data and comparison of the simulated results with historical records and present bank morphology. We calibrated the J&P model to the Quinn River using two approaches: (1) by comparing the simulated and the observed 38 year channel migration pattern; and (2) by comparing the correlation of the ratio of simulated inner- and outer-bank velocity to the ratio of observed left and right bank slope. We also compare the flow patterns predicted by the J&P model to results from 3D flow modeling using Delft3D (Roelvink and van Banning, 1994) at locations where the J&P model performed the poorest to study the differences in the flow field prediction between the two models.

Study site

The Quinn River flows through lacustrine sediments on the floor of paleolake Lahontan (Figure 1(a)) and is an atypical river in that the bed and banks are predominantly composed of silt/clay (Figure 1(b)) and that banks are free of appreciable vegetation or roots (Figure 1(c)). Vegetation not only adds heterogeneity to bank properties, but it also effects bank erosion processes through slump block formation and their subsequent erosion (Parker *et al.*, 2011). Coarse sand and gravel are not found in the study reach of the Quinn River because the low relief of the paleolake floor (channel gradient ~0.00015) prevents delivery of coarse sediments to the channel from the surrounding high-relief topography (Figure 1(d)). As a consequence, normal point bars or fixed or migrating alternate bars do not occur within the channel; rather, the bed is nearly flat but features steep cut banks and muddy inner banks with maximum slopes of 10–20° (Figure 1(c)). Because the high solute content of the sediments has made the region unsuitable for agriculture and because it is now protected as a wilderness area, there has been little direct human modification of the landscape. Although the Quinn River rarely receives direct rainfall and most of the major discharge events come from spring snow melt from the mountains, it has low flow throughout the remainder of the year which is most likely fed by groundwater. The Quinn River is still active and aerial photographs (1972, 1986, and 2006) show that significant channel migration including meander cutoffs have occurred in the past 38 years (Figure 1(e)).

Methods

Several methodologies were utilized to assess the ability of flow and bank erosion models to predict channel morphology and evolution in the Quinn River. These include: (1) modeling channel migration using the linearized J&P model; (2) comparative 3-D modeling using Delft3d; (3) correlation of the asymmetry of channel cross-sections with bend curvature and flow properties predicted by J&P and Delft3d; and (4) the relationship between inner bank profiles and migration rate.

Model description

The Howard (1992, 1996) implementation of the J&P model was used to simulate forward evolution of the Quinn River. The model uses a digitized initial channel centerline and channel gradient and cross-sectional properties to calculate the velocity distribution at each centerline location. In the J&P model channel width is assumed constant with vertical banks, and the bed is assumed to have a linear transverse slope. The result of interest in the flow modeling is the velocity perturbation at the bank, u_{1b}, defined as

$$u_{1b} = \frac{(u_b - U)}{U} \tag{1}$$

where u_b is the depth-averaged velocity near the bank and U is the mean velocity. As shown in Howard (1992) the velocity perturbation approximately equals the shear stress perturbation at the bank. We assume, as with most previous studies, that the bank erosion rate dn/dt is proportional to the velocity perturbation

$$\frac{dn}{dt} = 2Eu_{1b} \tag{2}$$

where E is the bank erodibility, which we determine through fitting (2) to observed long-term bank migration.

The downstream variation in flow properties in the J&P model is driven by the downstream changes in planform dimensionless centerline curvature, θ, which we measure in the nodal centerline representation as

$$\vartheta = 2W\psi/(d_u + d_d) \tag{3}$$

where ψ is the angular change in direction (positive for clockwise downstream turning at the node), W is channel width, and d_u and d_d are the distances to adjacent upstream and downstream nodes.

As suggested by J&P, the present modeling assumes bank erosion rates to scale linearly with the velocity perturbation, which would be zero for a long straight reach. Some field studies support this assumption (Ikeda *et al.*, 1981; Pizzuto and Meckelnburg, 1989; Constantine *et al.*, 2009). Simulated velocity varies linearly across the channel, and erosion is directed perpendicular towards the bank with the positive velocity perturbation.

The model was calibrated using field data such as meander wavelength, channel cross-sectional shape, and field measurements of flow resistance to find the model result that best matches the present channel centerline. The J&P flow model uses five parameters as input: the Froude Number, F, the channel width–depth ratio, γ, the coefficient of friction, $C_f = (U^*/U)^2$,

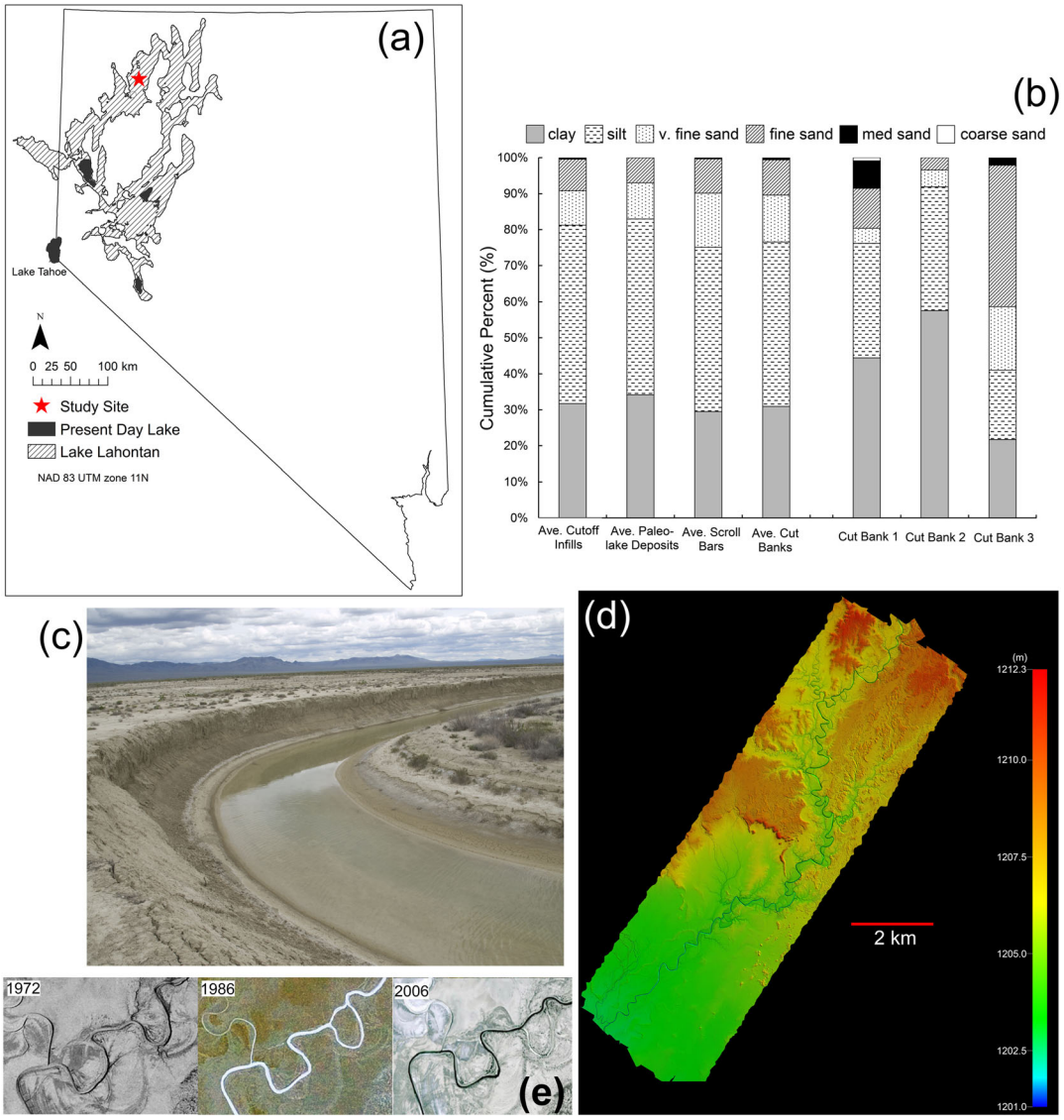

Figure 1. Location and characteristics of the study reach. (a) A map of Nevada showing the general location of the study area (Star) and the location of paleolake Lahontan (striped area). (b) Cumulative percentage graph of grain size distribution. Four left bars are averaged values for each depositional setting. Cut banks 1–3 are individual samples showing range of variability in cut bank samples. (c) A photo taken at the Quinn River showing sparse vegetation cover and asymmetry of the bank heights at a tight bend. (d) Detailed study reach covered by a 1 m LiDAR DEM. Overall relief of the area is ~11 m. Center of study region is at 41° 11′ 04.18″ N, 118° 45′ 25.75″ W. (e) Channel migration and chute cutoff from historical aerial photography for a reach near the northeast end of Figure 1(c). This figure is available in colour online at wileyonlinelibrary.com/journal/espl

where U is mean velocity and U^* is the shear velocity, a cross-sectional shape parameter, β, and an exponent relating velocity to bedload transport rate, M. For simulations involving the Quinn River in which bedforms are essentially absent, we only use the curvature-forced terms in the J&P model, so that the terms related to bars and sediment continuity and the parameter M are not required. Thus we utilize only the 'C' curvature-induced bed topography and flow perturbation terms in J&P and not the additive 'F' terms related to sediment continuity. The average spacing of centerline points used in the simulations was 13 m, about two-thirds of the estimated 20 m bankfull width.

Estimation of hydraulic parameters

A heavy winter mountain snowfall in 2010–2011 produced a long-duration peak flow through the study reach during the spring of 2011. A one-day field trip was conducted to collect flow data during this high flow in May 2011. The flow was about ¾ bankfull at the time of the visit. Roughness, width–depth ratio, and discharge at bankfull were estimated based on a May 2011 trip data and were used as initial input parameters to the J&P model. Flow measurements were made in the Quinn River using a Marsh-McBirney electromagnetic velocity meter at two locations: (1) about 40 km upstream from the study reach where the river flows through a culvert beneath the Leonard Creek Road; and (2) in the study reach at a previously surveyed cross-section. Because of the slippery bed and deep water, velocity measurements were not made at the center but as close to the center as possible. Given the slow change in the stage during the flood peak and the lack of major flow additions from tributaries between the culvert and the study reach, we assume that the discharge at the cross-section was the same as at the culvert. Measurements used to estimate the input parameters are summarized in Table I.

Flow properties were estimated in two ways. The first used measured velocity, hydraulic radius, and gradient to estimate Manning n and the friction factor C_f (Table I) The second used discharge, gradient, and flow cross-sectional area to estimate velocity and flow resistance (Table I, values in parenthesis). These methods provided nearly identical results. The surveyed cross-section was also used to estimate bankfull depth, and

Table I. Measured and estimated flow and channel properties for the Quinn River. The values in parenthesis were estimated using the discharge, gradient, and cross-sectional area (method 2)

Property	Units	At Observed Stage	Estimated Bankfull
Discharge, Q	$m^3 s^{-1}$	4.82	11.9
Mean Velocity, U	$m s^{-1}$	0.42 (0.36)	0.46
Mean Depth, H	m	0.85	1.29
Hydraulic Radius, R	m	0.87	1.32
Cross-sectional Area, A	m^2	13.4	25.78
Mannings n	$m^{1/6}$	0.027	0.027
Friction Coefficient, C_f	- -	0.007 (0.01)	0.008
Shear Stress, τ_0	$kg m^{-1} s^{-2}$	0.97	1.73
Shear Velocity, U^*	$m s^{-1}$	0.031	0.042
Froude Number, F	- -	0.14 (0.12)	0.13
Width/Depth Ratio, γ	- -	17.1	15.4

estimated flow properties assuming that Manning's n and the friction factor remain constant over discharge variations (Table I). Because even at the ¾ bankfull stage the flow was not carrying much sediment, we assume that the bankfull flow corresponds to the effective discharge for bank erosion and we utilize the estimates in Table I as the base values for a search for flow properties that best predict long-term channel migration and the downstream pattern of the asymmetry of cross-sectional shape. Also, bankfull discharge is commonly utilized as an approximation of an effective discharge for formation of channel geometry (Williams, 1978) and generally correlates well with channel dimensions (Richards, 1982). At flows greater than 12 $m^3 s^{-1}$ both flow modeling using Delft3d and HEC-RAS (USACE, 2010) showed appreciable overbank flow. No gauging stations exist for the Quinn River. Thus, we do not have the hydrologic record necessary to relate Quinn River morphology to frequency-based discharges (e.g. the mean annual flood).

Long-term analysis: fitting flow parameters to the observed 38 year migration pattern

The model was run using the 1972 centerline digitized from aerial photos (1:20500) and the hydraulic parameters estimated from the field data as starting conditions. The centerline for 2010 was created by tracing the center between estimated banklines three times using a 1 m resolution LiDAR DEM and averaging the three lines. The LiDAR was flown under low-water conditions (~ 15 cm depth at maximum) providing continuous coverage over the 10 km study reach (22.7 km channel length). We simulated channel migration to provide a best match to the 2010 centerline, and used the sum of the area between the resulting centerline and the actual 2010 centerline, A_l, as a measure of goodness-of-fit. The area includes underfit and overfit mismatches for both the left and right channel banks. Carrying the simulation forward, A_l decreases with iterations until the simulation projects too far into the future after which A_l increases (Figure 2(a), (b)). If not enough iterations have occurred, the simulated centerline has not migrated sufficiently from the initial centerline (Figure 2(c)).

We utilized the width to depth ratio, and the coefficient of friction as estimated for bankfull conditions (Table I) as initial assumed values, but explored the effect of slightly varying these parameters upon producing the best match to the 2010 digitized centerline (Figure 2(d)), hence the smallest A_l. The cross-sectional shape parameter, β, in the J&P model, however, is more difficult to define, because it is defined for alluvial channels with point bars. The cross-sectional bed slope in the J&P model is proportional to the dimensionless secondary current cell strength, δ_s, and a parameter X, which in turn is inversely proportional to β and the square root of the coefficient of friction. For a value of C_f =0.01 and β = 1.5 the value of X is 4.45, producing cross-section slopes similar to those observed in alluvial meandering channels (Johannesson and Parker, 1989). A nearly flat floor is obtained for large β. We tested two values of β, 1.5 which is the value suggested by J&P and a large value 150 corresponding to a gently sloping bed (X = 0.04). All of the parameters were varied with an assumption that the optimal solution occurs for those values corresponding to the smallest A_l.

Three meander chute cutoffs occurred within our study site during the 38 years. The simulation model can stochastically impose neck and chute cutoffs, but these would not necessarily occur in the same locations and times as the actual cutoffs occurring between 1972 and 2010. The occurrences of the cutoffs undoubtedly alter the migration pattern and thus incorporating cutoffs at the appropriate locations and timing is crucial to evaluating the model implementation. Low resolution aerial photography shows that all three cutoffs occurred around 1983, which we specify as the date of cutoffs.

In order to accurately place cutoffs, we first found the simulation parameters that resulted in the smallest A_l without cutoffs. Because time is not explicitly simulated we have calculated time in terms of iterations it took to reach the best-fit result. For example, the smallest A_l occurred at iteration 600 and thus in our simulation 600 iterations represent 38 years (Figure 2(a)). Assuming linear migration rate, we have performed two-stage simulations with an initial period starting from 1972 then imposing cutoffs around 1983 along the path suggested by the aerial photography and then continuing the simulation until 2010 using new erosion rate. We created cutoffs as straight lines approximating the course of the actual cutoffs.

Cut banks on the Quinn River are systematically steeper than inner banks and the two banks are relatively the same in steepness on straight reaches. In addition, at the locations where the migration has been inhibited over the years by impingement into the consolidated Lake Lahontan deposits, the height of the cut bank is much greater than the average bank height. To account for the effect of heterogeneity in the bank material on bank erosion rates, we have added a resistance factor to the original model. This is a similar idea to the bank erosion model proposed by Xu *et al*. (2011) except we used the average bank height to account for the resistant Lahontan deposit instead of water level as a reference level. We expressed the erodibility of the bank, ξ, as a function of the ratio, R, of the actual bank height to the mean bank elevation for the study area:

$$\xi = \xi_0 \ R^{-RF} (RF \geq 0) \tag{4}$$

$$R = H_b / E \tag{5}$$

where RF denotes how strongly bank height affects the erodibility (0 when bank height does not influence bank erodibility), H_b is the local height of the bank relative to the average relative bank elevation in the study area, E, and ξ_0 is the nominal bank erodibility estimated from the best-fit 38-year simulation with RF = 0. The R correction may jointly account for two factors leading to differences in bank erodibility: (1) higher banks imply more material must be removed per unit erosion perpendicular to the bank; and (2) higher banks generally expose the resistant Lake Lahontan sediments, whereas lower cut banks are generally formed in unconsolidated earlier inner-bank

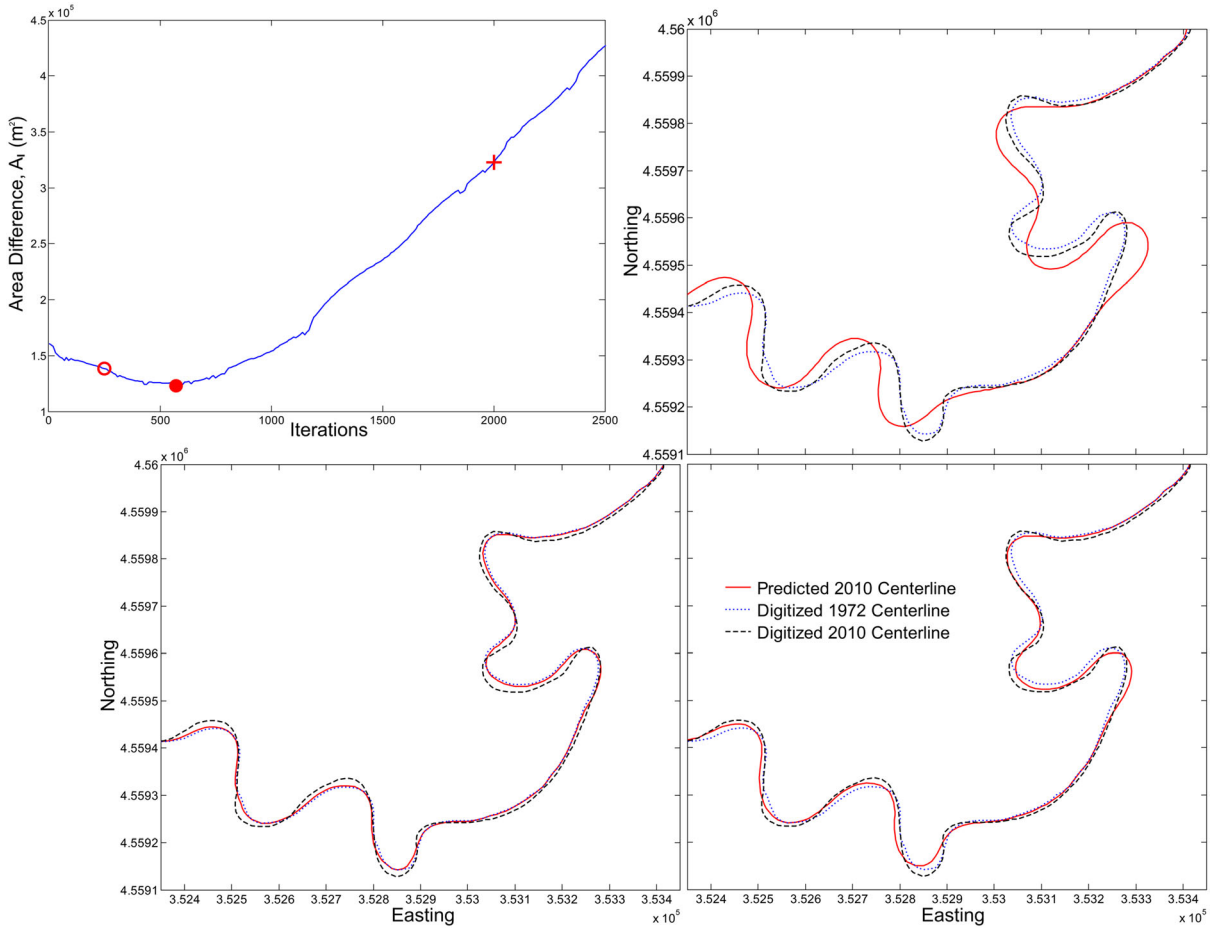

Figure 2. Modeling of 38 years of channel migration. (a) Temporal change of the area, A_I, between the simulated channel centerline and the 2010 actual centerline. The simulation starts from 1972 centerline and projects forward with each iteration. The smallest A_I value on this graph indicates the best match for the 2010 centerline. (b) The simulation result at point b on (a). The model has been projected too far in the future. The resulting centerline is passed beyond 2010 centerline. (c) Simulation results at point c on (a). Not enough time (iterations) has passed hence the simulated centerline (red) is closer to the initial 1972 centerline (blue) than to the 2010 centerline (black). (d) The simulation result that gave the smallest A_I value, hence the best match to the 2010 centerline. AD83 UTM Zone 11 N is used for (b)–(d), with flow from upper right to lower left. This figure is available in colour online at wileyonlinelibrary.com/journal/espl

deposits of the modern Quinn River. For this study we used four different RF values (0, 1, 2, and 3).

Flow modeling using Delft3D

Because of the limiting assumptions of the depth-averaged, linearized J&P flow model, we have modeled flows and bank stresses over the study reach using Delft3D, a fully 3D model that has recently been released as open source (Roelvink and van Banning, 1994). We used the LiDAR DEM to generate the bed topography. Because water depths when the LiDAR was taken were less than 15 cm and water was stagnant, the topography adequately represents the channel geometry at bankfull flows. We have simulated flow through the entire 22.7 km reach covered by the LIDAR DEM as well as exploratory runs in a 2.5 km reach that contains two sharp bends (locations 5 and (b) on Figure 3) where the river impinges upon the Lake Lahontan sediments as well as several more typical bends (Figure 3). This reach also contains a bend whose migration rate is strongly underpredicted by the J&P model (as discussed below).

As an initial step, we used cross-sections spaced 20 m apart created from the LiDAR DEM as input to HEC-RAS 4.1.0 (USACE, 2010) to model the water profile along the river to define initial flow depth required for Delft3D assuming an effective discharge of 12 $m^3 s^{-1}$ and a Manning's coefficient, n, of 0.03. The RGFGRID module within the Delft3D user interface was used to create a conformal flow grid for the reach in which grid lines cross the channel approximately normal to the flow and follow the curving channel downstream. For the simulations of flow through the entire reach this resulted in a grid 20 cells across and 4376 cells downstream averaging about a 1.2 m resolution cross-stream and 5.2 m downstream. For exploratory runs we simulated the reach shown in Figure 3 with a 20 by 518 cell grid with the same resolution. About 11 grid cells were in the main channel and the remainder extended onto the shallow flow on the upper banks. The LiDAR DEM was then interpolated onto the grid using the Delft3D QUICKIN module. We used 10 vertical layers with a logarithmic spacing (as suggested in the Delt3d documentation), a k-Epsilon model for 3D turbulence and a 1.0×10^{-6} $m^2 s^{-1}$ assumed horizontal eddy viscosity. The k-Epsilon turbulence closure is the most advanced turbulence model in Delft3D, and widely used for simulating fluvial flows (Edmonds and Slingerland, 2008; Luppi *et al.*, 2008) and predicted flow properties in sharp bends compare well with laboratory flow measurements (van Sabben, 2010). Exploratory runs indicated that the flow converged to steady values in 3 h for the 2.5 km reach and 2 days for the 22.7 km reach, which we used for subsequent simulations. Time steps varied from 0.1–0.01 min per iteration. Several runs were made adjusting the downstream water level elevation to achieve a smooth water surface profile approximating the water surface gradient calculated by HEC-RAS. In exploratory simulations we varied the bed/bank roughness between

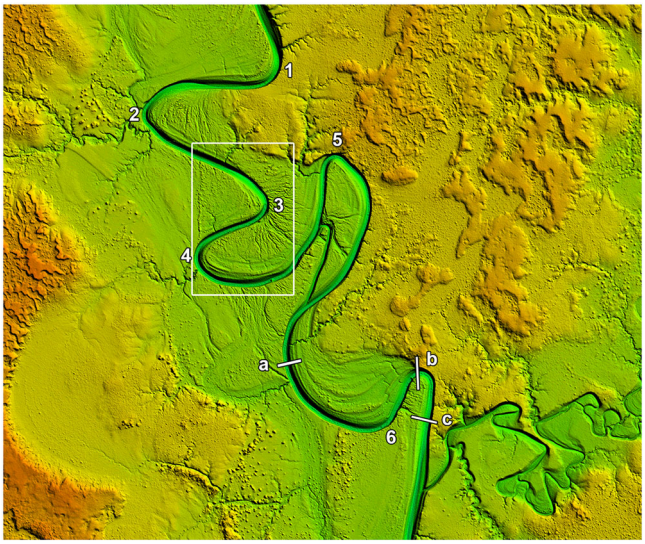

Figure 3. Reach selected for detailed study (centered at 41° 11′ 37.91″ N, 118° 44′ 27.70″ W). Shaded relief of the channel and floodplain (total relief about 3.5 m). Lines crossing the channel (a, b, and c) correspond to Figure 9. The two sharp bends occur where the channel impinges upon higher banks of partly consolidated Lake Lahontan sediment (locations 5 and b). Numbers refer to individual locations of bends shown in Figure 5. Letters a–c refer to cross-sections shown in Figure 9 and the box shows location of Figure 10. Flow from top to bottom. This figure is available in colour online at wileyonlinelibrary.com/journal/espl

$n = 0.02$ and $n = 0.04$, simulations assuming no-slip and free lateral boundaries, and a few simulations using the subgrid scale Horizontal Large Eddy Simulations (HLES) with assumed relaxation times from 1 to 10 min. We also simulated flow patterns for discharges up to 15 $m^3 s^{-1}$ using a 50x686 grid for the 2.5 km reach. The results from the exploratory simulations show that $n = 0.03$ and horizontal eddy viscosity of 1×10^{-6} $m^2 s^{-1}$ gives the best-fit result for the Quinn River.

For the Delft3d flow modeling we defined a measure of cross-sectional bed shear stress asymmetry, *rskew*, analogous to the velocity perturbation in the J&P model.

$$rskew = (x_\tau - \overline{x})/(x_L - x_R) \tag{6}$$

where x_L and x_R are the locations along the cross-section of the left and right banks, respectively, $\overline{x}$ is the midpoint between x_L and x_R, and x_τ is calculated as

$$x_\tau = \frac{\sum x_i w_i \tau_i}{\sum w_i \tau_i} \tag{7}$$

where the summation is taken over all grid cells from the left bank to the right bank and x_i is the cell location along the cross-section, w_i is the width of the cell, and τ_i is the bed shear stress magnitude at that cell.

Short-term analysis: fitting the flow parameters to present bank asymmetry

A second method of calibrating and testing the applicability of the J&P and Delft3d models is to examine the correlation between the predictions of the flow models in relation to the downstream variation in the cross-sectional shape and width of the channel. The channel cross-sectional shape and channel width should respond to the flow pattern in meander bends after a few meters of lateral migration relative to the multi-decade lateral migration of the channel which is often tens of meters. Thus we hypothesize that the cross-sectional channel characteristics should be closely related to flow parameters predicted by the present channel pattern.

In natural meandering channels, the eroding bank is generally steep as a result of undercutting and the prograding opposite bank is gentler. This pattern was observed in the Quinn River as well. We characterize this using an *asymmetry parameter*, B_a, defined as:

$$B_a = \ln\left(\frac{S_{L\max}}{S_{R\max}}\right) \tag{8}$$

where S_{Lmax} is the maximum bank gradient on the left bank, and similarly for S_{Rmax} on the right bank. Thus portions of the channel with steeper left banks are positive, and negative for the opposite asymmetry. We quantify this by constructing cross-sections perpendicular to the channel centerline at each sample location and use the LIDAR DEM data to determine gradients. From the centerline a search progresses outwards along the cross-section towards both the left and right banks and the maximum gradient on each bank is noted.

The cross-section properties and the J&P and Delft3D flow properties are defined for each of the 4376 sample locations along the channel. This data series was analyzed using the Matlab® tstool for time series analysis (where here downstream distance takes the place of time). The degree of correspondence between any two model prediction and cross-section properties is measured by the cross-correlation for a range of positive and negative lags between the two data series. A cross-correlation at lag zero is between two data series taken at the same locations. A lag one cross-correlation is between one data series and the comparison data series separated by one upstream cross-sectional location. The expectation is that if the J&P or Delft3D models for bank erosion are valid and the input parameters for the model are correctly chosen, then the bank asymmetry ratio and the near-bank shear stresses should have high correlation at close to zero lag. The degree of cross-correlation should diminish steadily with larger lags (both positive upstream and negative downstream). We examine the cross-correlation, r, and the downstream lag, L, between the bank asymmetry parameter, B_a, the velocity perturbation and *rskew* from the model results, and bend curvature estimated from the channel centerline. A similar analysis examined channel width in relation to the absolute values of curvature and flow asymmetry, using the distance between the maximum gradient locations on the left and right banks as the measure of channel width. We use this geometric definition rather than a bankfull width which is more difficult to define objectively.

The cross-correlation time series analysis tests which values of the input parameters give the best fit to the observed variation in bank asymmetry. This is a parallel, but independent method from modeling long-term migration, of finding the most appropriate model parameters for the J&P and Delft3d models.

Inner-bank and floodplain profiles

To investigate the effect of migration rate on the shape of inner banks we constructed cross-sectional profiles across the Quinn River inner bank and floodplain deposits. The term *inner-bank* refers to the depositional sequence opposite cut banks as opposed to the usual usage of point bar. The term point bar generally implies a curvature-forced bar of cohesionless sediment, whereas the inner banks of Quinn River meanders are steep (~15° maximum slope) and composed of muddy drape deposits. Although sedimentation on the inner banks is dominated by silt and clay deposited by oblique accretion (Page

et al., 2003), the silt/clay drapes are often mantled on the upper banks and floodplain by silty-sand scroll bars (e.g. on the bank opposite '6' in Figure 3).

Using the LiDAR DEM, 238 profiles were measured along the 22.7 km study reach. They were measured perpendicular to the channel centerline at locations where migration direction inferred from meander scrolls was nearly parallel to the migration direction and where the scroll bar complexes were at least 50 m wide. The profiles were adjusted to zero elevation at the channel centerline and grouped according to local channel migration rate and profiles in each migration rate group were averaged to give representative profiles from the channel centerline across the inner bank.

Results

Long term: plan form evolution

The J&P model did a good job of projecting 38 years of migration after making slight modifications of the estimated simulation parameters (Figure 2(d)). After the implementation of three cutoffs, the model resulted in the best fit area difference, A_l, of 0.12 km^2. The one input parameter we changed from the initial assumed values was the cross-sectional shape parameter, β, from 1.5 to 150 (Table II, "Fitting migration pattern"). The use of the resistance factor *RF* set to a value of 3.0 was effective at slowing erosion at locations where the channel was pinned against the original Lake Lahontan deposit (Figure 4(a)). Without the resistance factor, the channel was predicted to migrate farther than observed when in reality migration is inhibited due to the resistant bank (Figure 4(b)).

At two locations the model simulation and the digitized 2010 centerline had the greatest disparity. In both cases the channel migrated more rapidly than predicted based on the overall best fit. One of the two locations was given further attention because of its unique setting (locations '6' and 'X' in Figures 3 and 4, respectively). It is just upstream of where the Quinn River encounters resistant Pleistocene lake beds and forms a very tight bend that is nearly immobilized. At tight bends such as this one, hydrodynamics of the flow would be more complicated (Blanckaert, 2009, 2011; Ottevanger *et al.*, 2012) and the linear J&P model would estimate velocities poorly, resulting in inaccurate predictions of planform evolution.

Table II. Best-fit model parameters for migration modeling using Johannesson and Parker (1989)

	F	C_f	γ	β	n (m$^{1/6}$)
Fitting migration pattern	0.14	0.008	15.4	150	0.03
Fitting bank asymmetry	0.13	0.012	15.4	1.5	0.03

Short term: bank asymmetry and channel width

The relationship between bank asymmetry, planform curvature, and modeled channel flows was explored through the 22.7 km river reach. Results for the 2.5 km reach in Figure 3 are shown in Figure 5 for the optimal flow simulation parameters (as discussed below). Variables in this plot have been smoothed by a 9-point moving average because of high-frequency variations introduced as a result of discretization of channel planform and cross-sectional geometry. The maxima and minima of bank asymmetry B_a systematically lag downstream from the corresponding curvature fluctuations, θ. The modeled variation

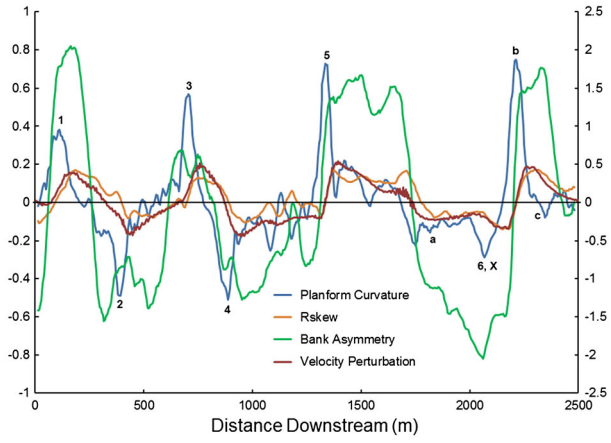

Figure 5. Variation in channel and flow properties in the channel reach shown in Figure 3. Vertical scales for plots: dimensionless curvature (θ) (right axis); *rskew* (left axis), cross-sectional asymmetry, B_a (right axis). Velocity perturbation, u_{1b} (right axis). Numbers and letters refer to locations on Figure 3. This figure is available in colour online at wileyonlinelibrary.com/journal/espl

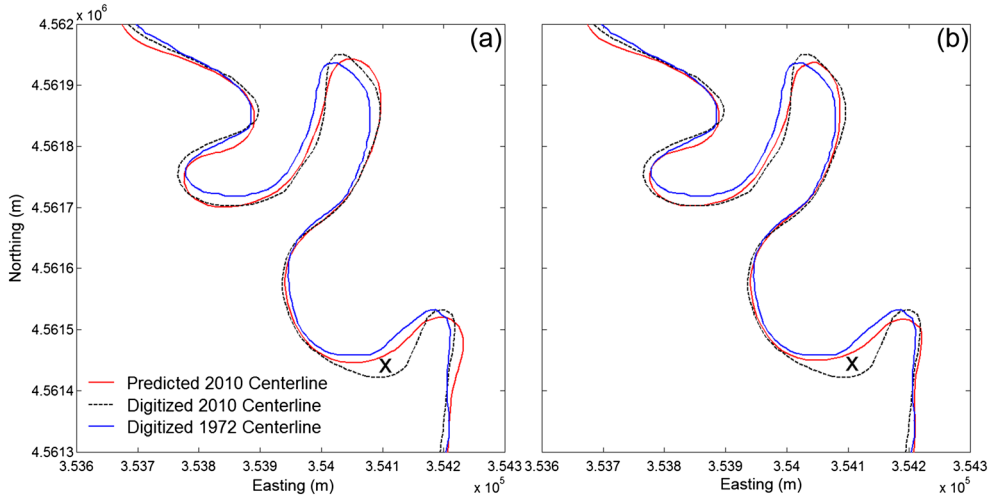

Figure 4. Effect of including a bank resistance coefficient based upon cut bank height. (a) Simulation with correction for bank height. (b) 1972, actual 2010 and predicted 2010 centerline without correction for variable bank height. This channel section is located within the region shown in Figure 3. Both (a) and (b) are shown in NAD83 UTM Zone 11 N. Location 'X' is at a reach where the rate of migration is strongly under-predicted by the J&P model. Flow from top to bottom. This figure is available in colour online at wileyonlinelibrary.com/journal/espl

in the velocity perturbation u_{1b} closely follows B_a but with a slight offset downstream. The bed shear stress asymmetry *rskew* from the Delft3d simulation exhibits a pattern nearly coincident with the J&P velocity perturbation.

These patterns were expressed quantitatively as spatial cross-correlations between the variables. Figure 6 shows the cross-correlation between velocity perturbation u_{1b} and the bank asymmetry B_a for the J&P flow model for two different assumed values of the coefficient of friction, C_f. Positive lags correspond to correlations between B_a and upstream values of u_{1b}. In this analysis data points are separated by 19 m, so that the observed peaks correspond to lags of about 9 and 28 m for C_f of 0.012 and 0.006, respectively. That is, the best correlations occur between values of local values B_a and values of u_{1b} located several meters downstream. Similarly, Figure 7(a) shows the cross-correlation between the slope asymmetry, B_a, and *rskew*. For the Delft3d simulations grid cells are spaced 5.2 m apart, so that the observed maximum correlation occurs as a negative lag of about 25 m. Both the J&P and Delft3d models exhibit strong maximum correlations ($r \sim 0.7$) between observed bank asymmetry and predicted flow asymmetry as measured by

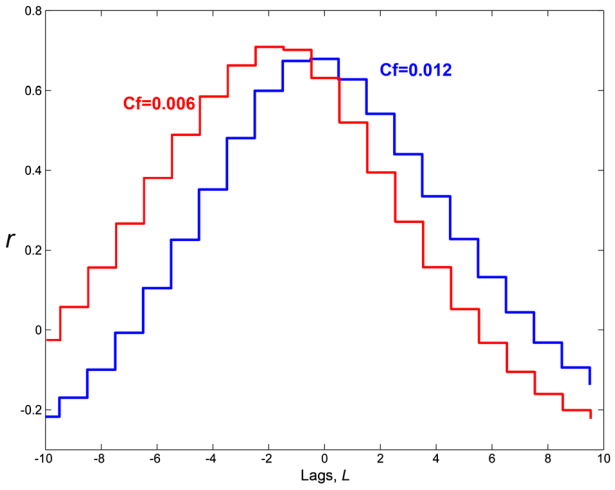

Figure 6. Cross-correlation between simulated near-bank velocity perturbation, $u_{1b,}$ calculated by the J&P model (1989) and the channel cross-sectional asymmetry, B_a, for the entire 22.7 km channel. Correlation shown for two assumed values of the coefficient of friction, C_f. Individual spatial lags on the horizontal axis correspond to 19 m of separation. Positive numbers reflect correlations of B_a with upstream values of u_{1b}. This figure is available in colour online at wileyonlinelibrary.com/journal/espl

u_{1b} and *rskew*, respectively. In contrast, the maximum flow velocity on the outside of a bank is delayed downstream from the location of maximum bend curvature in natural streams, a pattern which is predicted by both the J&P and Delft3d models. Maximum cross-correlation of B_a with curvature θ occurs at about 42 m upstream (Figure 7(b)).

Cross-correlations were examined for a variety of assumed parameter values for the J&P model ranging from the nominal values in Table I. The optimal values that are plotted in Figure 7 are not much different from those of Table I, such that $\gamma = 15.4$, $F = 0.13$, $C_f = 0.012$, and $\beta = 1.5$ (Table II, "Fitting bank asymmetry"). Similarly a range of flow simulations were conducted with Delft3d, with flow resistance, n, between 0.02 and 0.04 and with and without HLES modeling. The resulting lag correlations between channel properties and flow properties calculated by Delft3D changed little for different model assumptions, and Figure 7 shows results from parameterization with $n = 0.03$, background horizontal viscosity of 1.0×10^{-6} m^2 s^{-1} and the k-e turbulence model.

We also investigated whether the channel width varies systematically with position within bends. Because width is always positive, it is correlated against the absolute values of the velocity perturbation u_{1b}, the average bed shear stress from the Delft3d model, and the absolute value of the dimensionless planform curvature. A modest negative correlation (−0.35) occurs for width versus absolute planform curvature measured about 45 m upstream (Figure 7(c)), and a strong (−0.6) negative correlation occurs for width versus average bed shear stress in the Delft3d modeling at a downstream lag of 11 m (Figure 7(d)).

Bank profiles related to channel migration rate

Figure 8 shows profiles of inner bank topography grouped and averaged by local channel migration rate, m. Channel width from the centerline and inner bank profiles are remarkably consistent across the range of migration rates. The only systematic trend is that the elevation to which inner bank elevations become asymptotic is lowest where migration rates are highest. The independence of bank profiles to the migration rate implies that sedimentation rates scale proportionally to migration rate and that inner banks are represented by a simple equilibrium profile, at least for the Quinn River system. The profiles also demonstrate that almost all of the inner-bank deposition occurs as a bank drape and that deposition beyond the first 15 m from the thalweg is minor.

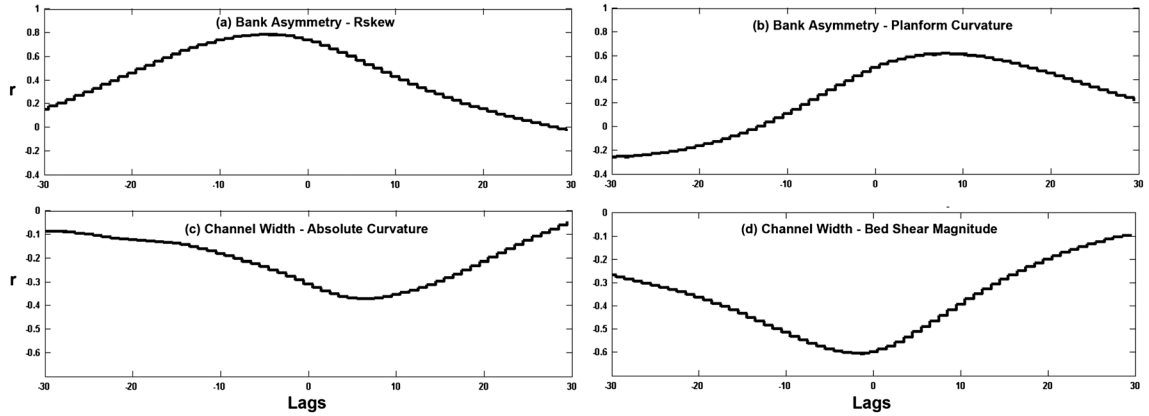

Figure 7. Cross-correlations between channel properties and flow properties calculated by Delft3D for the entire 22.7 km channel. Positive numbers refer to correlations between channel property and second variable measured at upstream locations. One lag length equals 5.2 m: (a) cross-correlation between cross-sectional bank asymmetry, B_a and *rskew*; (b) cross-correlation between, B_a, and absolute values of planform curvature, ϑ; (c) cross-correlation between channel width (measured between the maximum bank slopes on left and right banks) and absolute ϑ; (d) cross-correlation between width and absolute value of average bed shear stress.

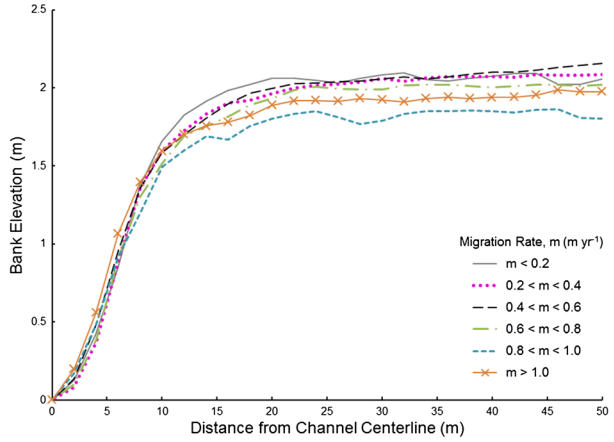

Figure 8. Profiles across inner bank deposits of the Quinn River grouped by average channel migration rate over the 38 year record (rates in m yr^{-1}). This figure is available in colour online at wileyonlinelibrary.com/journal/espl

Flow patterns in Delft3D

Flow properties simulated by Delft3d are shown in Figure 9. The top row relates to a cross-section taken across a long, gently curved meander (location a in Figure 3). The profiles are portrayed looking upstream. Both the bed topography (blue in Figure 9a1) and the bed shear stress (red) exhibit skewing towards the outer bank. A well-developed secondary circulation is present with downward flow near the outer bank (Figure 9a2). Slight reverse vertical eddies occur near the surface close to the inner and outer banks (Figure 9a2). The turbulent kinetic energy ($m^2 s^2$) likewise is strongest near the eroding outer bank (Figure 9a3) where the velocity gradients are greatest. Location b is located near the start of a strong clockwise planform bend, where the river is incising into relatively resistant lake-bed sediment. The sense of secondary circulation has responded rapidly to the change in curvature, with downwelling near the outer bank (Figure 9b2). Such rapid response is also predicted by the J&P model. The shear stress and maximum turbulent energy, however, are still concentrated along the inner bank (Figure 9b1 and b3), inherited from the upstream bend with opposite curvature. By 104 m downstream at location c the maximum bed shear stress and the maximum of the turbulent energy have shifted to the outer bank (Figure 9c1 and c3), although the strong clockwise secondary circulation is limited to the region close to the outer bank (Figure 9c2).

Discussion

This study demonstrates the ability of a simplified meander flow model to predict long-term migration pattern as well as bank

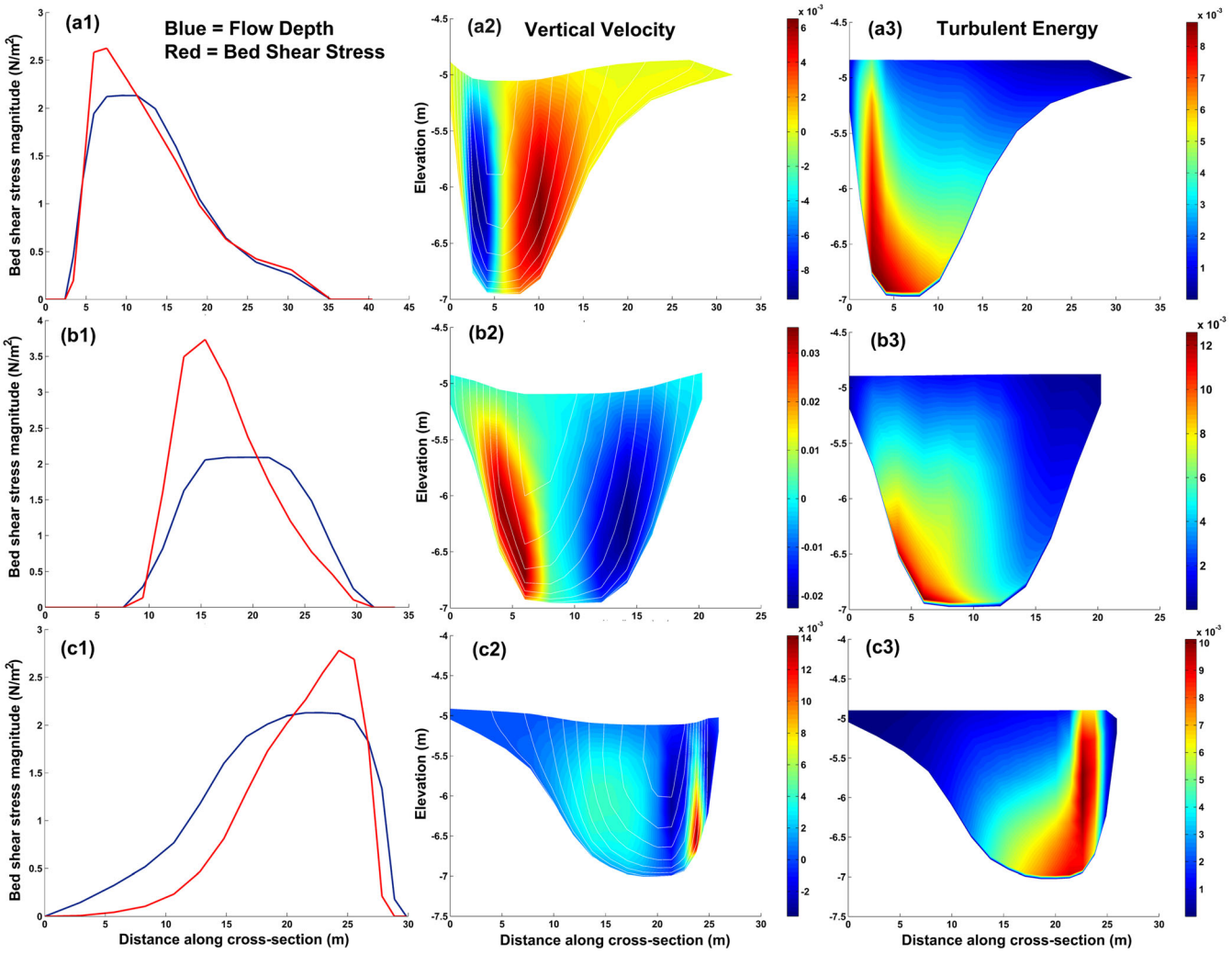

Figure 9. Simulated flow properties from D3D at the three cross-sections shown in Figure 3. (a1, b1, and c1) flow depths (m) and bed shear stress (N m^{-2}) for the cross-section. Both plots refer to the numerical scale but with different units. (a2, b2, c2) Secondary flow magnitude (m s^{-1}) with superimposed contour lines for downstream flow velocity. Maximum contour of downstream flow is 0.6 m s^{-1}. (a3, b3, c3) Turbulent flow intensity ($m^2 s^{-2}$). This figure is available in colour online at wileyonlinelibrary.com/journal/espl

asymmetry for a mud-dominated channel using input values estimated from field data. Strong correlation was observed between the bank asymmetry and the velocity asymmetry. The unexplained variability probably results from poor representation of the flow in sharp bends and variations in bank properties not reflected upon bank height. Small deviations of the predicted 2010 centerline from the actual path are found throughout the reach and in a few locations the migration is strongly over- or under-predicted. These discrepancies might originate from several causes, including the choice of migration rate law, inadequacies of the flow model, and spatial variation in bank properties.

Models of meander evolution have assumed that the rate-controlling factor is the ability of the flow to erode the cut bank and remove the resulting debris (bank pull) (Parker *et al.*, 2011). Clearly, however, if sedimentation on the inner bank lagged outer bank erosion, velocity would slow and migration might halt. The flume experiments of Braudrick *et al.* (2009) demonstrate the importance of fine sediment point bar deposition in initiating and sustaining a meandering pattern. So it remains an open question whether inner-bank deposition might dictate migration rates (bar push) (Parker *et al.*, 2011).

The negative correlation between the channel width and shear stress indicates that the river is narrowest when the velocity perturbation is strongest and the cross-section is most asymmetrical (Figure 7). A widening of the channel in the straight reach downstream from location c in Figure 3 is clearly visible. Systematic variations of channel width between straighter crossings and bends have been observed elsewhere, usually in the pattern noted here with narrower cross-sections in bends, but with the inverse case in wide rivers with prominent point bars (Luchi *et al.*, 2011, 2012; Frascati and Lanzoni, 2013). In the Luchi *et al.* (2011) model width variations occur due to the necessity for sediment transport capacity to remain constant through changes in bar topography associated with bends. Because the Quinn River lacks point bars in the classic sense, the cause for systematic width variation presumably relates to some other interaction of flow structure with sedimentation processes such as secondary circulation advecting suspended sediment to the inner bank (Nanson, 1980).

The observation that channels are narrowest in sharp bends (Figure 7) could be an argument for bar push in that narrow channel segments might correlate with fast flow and rapid bank erosion. Flow modeling with Delft3D at the slightly overbank stage of 15 $m^3 s^{-1}$ shows strong, advective interchange of main channel flow with flow over the surrounding floodplain downstream of elongated bends at bankfull conditions (Figure 10), suggesting curvature-dependent delivery of sediment to the floodplain. On the other hand, the observation that inner bank profiles are essentially independent of migration rate (Figure 8) suggests that inner bank sedimentation in the Quinn River can keep pace with channel migration and that the rate-controlling factor in channel migration is bank erosion (bank pull) as is assumed in most meander evolution modeling. However, this uniformity of inner bank profiles may be attributed to relatively low migration rate. Deposition at the inner bend does not start to lag outer bank migration until the erosion rate at the outer bank is sufficiently high (Engel and Rhoads, 2012). The strong correlation between channel asymmetry and asymmetry of shear stress also provides support for bank pull as the controlling factor (Figures 6 and 7).

Modeling of bank erosion has generally assumed a linear relationship between the velocity perturbation and rate of bank erosion. Some field studies support this assumption (Pizzuto and Meckelnburg, 1989; Constantine *et al.*, 2009). We tested the effects of two alternatives to the linear bank erosion rate law. The first was a non-linear dependency of bank erosion rate

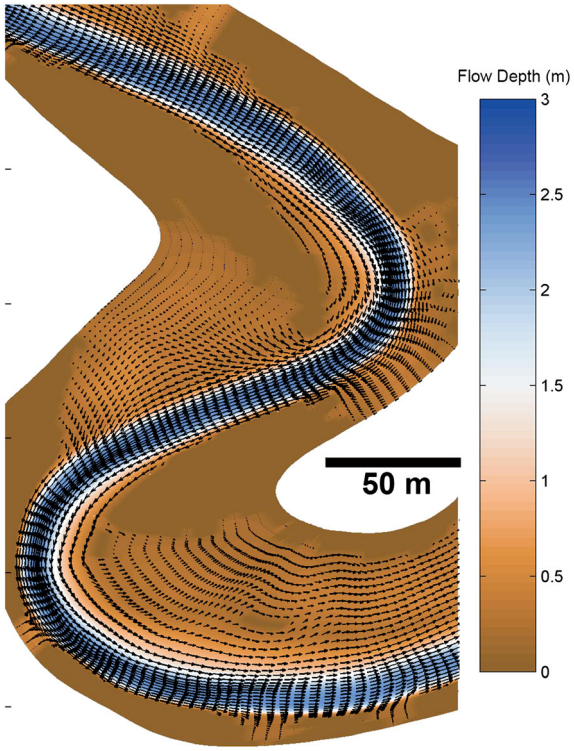

Figure 10. Depth-averaged flow magnitude and direction for the sinuous bends in the box shown in Figure 3. Simulation using Delft3D for 15 $m^3 s^{-1}$. Colors show flow depth (m). Longest arrows (within main channel) correspond to about 0.65 $m s^{-1}$. Note strong advective flow exchange between the main channel and low-lying portions of the floodplain. Dark brown areas not flooded. This figure is available in colour online at wileyonlinelibrary.com/journal/espl

on the velocity perturbation, specifically a square and a square-root dependency. Neither of the non-linear rate laws provided as good a fit to the 2010 meander planform as the linear assumption. Howard (1992) suggested a critical shear stress for bank erosion might be appropriate for strongly cohesive banks and the effects of such a critical stress has been explored by Motta *et al.* (2012). The pattern of migration resulting from such an assumption features bulbous meander loops and sharp bends, which is observed in some meandering streams (Motta *et al.*, 2012). However, the Quinn River meanders do not exhibit this shape, having a more sinusoidal planform except where impinging on resistant banks (Figure 3). Inclusion of a critical shear in the present model reduced the accuracy of the simulated fit to the 2010 centerline. Therefore the linear bank erosion rate law appears to provide the best match to observed bank migration.

The model utilizes a depth-averaged flow parameterization and assumes a simple cross-sectional geometry with a constant channel width and moderate bend curvature. As such there are circumstances where the linearity assumption becomes inaccurate. We investigated this possibility through comparison of the J&P flow modeling with comparative simulations using Delft3D. Both models predicted a similar pattern of shear stress asymmetry to curvature forcing (Figure 5). Modifications to the 1D flow parameterization have been presented which address flow in sharp bends (Blanckaert and de Vriend, 2010; Ottevanger *et al.*, 2012). Observations and theoretical modeling suggest sharp meanders may develop secondary flows on the inside or outside banks (Blanckaert, 2009, 2011; Ottevanger *et al.*, 2012). Delft3D modeling of the flow in the sharp bends did not show such secondary flows (Figure 9). Outward migration in smooth, sharp bends of the Quinn River may essentially cease prior to developing secondary flows as near-bank shear stresses diminish with increased curvature.

Both the J&P and Delft3D cross-correlations between bank asymmetry and flow asymmetry indicate a downstream lag of 10–25 m in the maximum correlation (Figures 6 and 7). This might reflect somewhat inaccurate estimates of flow properties in the simulation modeling, but another factor may explain all or part of this delay. The migration of meanders involves both enlargement and downstream translation (Ikeda *et al.*, 1981). Portions of cut banks no longer being undermined may persist as steep slopes for a period of time after bends migrate downstream. This is evident in the sharp bends at locations 5 and b in Figure 3, where the migration path of the bend apex is evident as relict steep slopes. This means that our initial hypothesis that bank asymmetry reflects only present flow properties is somewhat in error, i.e. there is a temporal memory in the spatial structure of bank asymmetry.

The J&P model-predicted centerlines deviated substantially from the 2010 centerline in a few locations. One location in particular is the broad bend (at '6' and 'X' in Figures 3 and 4, respectively). Neither the J&P model nor Delf3D predicted strong outer-bank velocity perturbations at this locality (between locations a and b in Figure 5). This suggests that spatial variations in bank properties may account for discrepancies between model predictions and observed rates of bank retreat.

We observed two dominant types of bank stratigraphy along the Quinn River within the study reach. The first is where banks cut into the moderately consolidated Pleistocene deposits of Lake Lahontan (e.g. along the near left bank in Figure 1(c) and at locations 5 and b in Figure 3). These banks are typically steeper and higher than elsewhere, and a resistance factor based upon relative bank height successfully accounted for reduced migration rates along such banks (Equations (4), (5) and Figure 4). Along much of the study reach the river is reworking inner bank deposits. Such banks are dominated by mud (Figure 1(b)), but contain layers varying in percentage of clay, typically dipping 5–20°. The cut banks incise these beds at various orientations relative to the strike of the deposits. At the two locations where bank migration rates are strongly underestimated (including at '6' and 'X' in Figures 3 and 4, respectively), the cut banks are nearly normal to the strike. This may be the most favorable orientation for bank erosion, because erosion of the more friable sandy-silt layers may undercut the more coherent clay-rich layers (Figure 1(b)). Conversely, where exposed older bank deposits dip towards the present bank, erosion through mud drapes may be inhibited and migration rates reduced. We conclude that spatial variations in cut bank erodibility are likely to be the dominant cause of significant variations in bank migration rates not accounted for by simulation modeling.

A final mechanism that may influence bank erosion rates is the effect of very large flood flows (15–30 $m^3 s^{-1}$) that occur on decadal time scales. During such flows extensive flooding occurs across the floodplain (Figure 10), and, as is evident in Figure 3, the floodplain surface is sculpted into small scours as well as broader flood chutes incised to various depths. The sparseness of vegetation and high erodibility of the fluvial deposits contributes to the extensive floodplain scour. Chute cutoffs dominate along the Quinn River, and occur during the intense flood events. The overbank floods and in-channel flows may possibly interact during such floods, creating, for example, vortices that locally accelerate bank erosion.

Conclusions

The Quinn River lacks coarse sediment in both the channel bed and the banks and lacks vegetation on banks. Sediment samples collected from the study area were composed of at least 40% silt and clay with some consisting entirely of silt and clay. As a result, Quinn River does not have typical point bars that are composed of bedload sediment. Instead fine sediments are deposited as mud drapes and overbank flow deposits. This lack of classic point bars gives Quinn River a canal-like form with a flat channel bed and relatively steep banks. The simple linearized J&P flow and bank erosion model can successfully replicate the migration pattern of this mud-dominated channel, which has no appreciable vegetation on banks, over multi-decade periods using the flow parameters measured in the field. An independent application of the model to predict bank asymmetry yielded similar results for the best fit parameters indicating that the bank asymmetry is a good indicator of corresponding flow asymmetry leading to bank erosion.

The model was modified to allow bank erodibility to decrease or increase with relative bank height. This modification gave better prediction of actual migration in areas where channel was cutting into the resistant Lake Lahontan sediments. However, the modified model was not effective in explaining the areas of rapid migration (mainly where channel is cutting into its former inner bank deposits) because, unlike the Lahontan deposits characterized by large bank heights, the presence of old inner bank deposits is not reflected in bank height variations.

In sharp bends the assumptions of the 1D linearized models such as J&P become inaccurate (Camporeale *et al.*, 2007; Blanckaert and de Vriend, 2010). Patterns of flow asymmetry in the sharpest bends of the Quinn River, however, are nearly identically predicted by the J&P model and the more general Delft3D model. The lack of bedforms and flat bed of the Quinn River may lessen the effects of flow non-linearity. As a result, the simplified and rapidly-computing J&P model is likely to be a useful tool to estimate erosional forces for prediction of future channel migration in the canaliform, mud-dominated Quinn River. This is tempered, however, by the obvious influence of spatial variations in cut-bank properties on migration patterns. Although the effects of inhomogeneous bank properties on meander evolution have been examined in theoretical simulation modeling (Howard, 1992, 1996; Sun *et al.*, 1996; Güneralp and Rhoads, 2011), geotechnical characterization of bank properties in natural streams sufficient to accurately predict long-term, large-scale migration is likely to be a formidable undertaking, not only for the Quinn River, but as a general issue (Güneralp and Marston, 2012).

Meander migration models generally assume that the rate of migration is proportional to the maximum bank shear stresses. But sedimentation rates on inner-bank must keep pace with bend migration, raising the possibility that inner-bank deposition (bar push) rather than cut bank erosion (bank pull) governs migration rates. Topographic profiles across inner banks are essentially invariant over a wide range of migration rates, implying that sediment deposition rates on inner banks increases in proportion to migration rate. This suggests that the traditional formulation that cut bank erosion processes govern migration rates is appropriate for the Quinn River.

Although inner bank deposition keeps pace with cut bank erosion over decadal time scales, cut bank erosion may dominate during rising and high flow stages, whereas deposition is most likely during waning flow stages. Thin mud drapes commonly mantle the more gentle cut banks when observed at low flow conditions, suggesting falling-stage deposition. However, direct observations of stage-dependent erosion and deposition are lacking. Future work will focus on depositional processes and the sedimentology of the Quinn River.

Acknowledgements—This research was supported by National Aeronautics and Space Administration Grant NNX09AM02G to A. Howard and a National Science Foundation National Center for Airborne Laser

Mapping seed grant to Y. Matsubara. The authors are indebted to the following for discussions and field assistance: D. M. Burr, C. A. Braudrick, W. E. Dietrich, C. Dufurrena, S. A. Drummond, M. G. Kleinhans, J. M. Moore, A. Morgan, E. Mosselman, W. Ottevanger, M. Palucis, G. Parker, and R. M. E. Williams. Research was conducted under a permit from the US Bureau of Land Management. The paper was substantially improved by comments by Bruce Rhoads and the anonymous reviewer.

References

Blanckaert K. 2009. Saturation of curvature-induced secondary flow, energy losses and turbulence in sharp open-channel bends: laboratory experiments, analysis, and modeling. *Journal of Geophysical Research* **114**: doi:10.1029/2008JF001137.

Blanckaert K. 2010. Topographic steering, flow recirculation, velocity redistribution, and topography in sharp meander bends. *Water Recources Research* **46**: W09506. doi:10.1029/2009WR008303.

Blanckaert K. 2011. Hydrodynamic processes in sharp meander bends and their morphological implications. *Journal of Geophysical Research* **116**: F01003. doi:10.1029/2010JF001806.

Blanckaert K, de Vriend HJ. 2010. Meander dynamics: a nonlinear model without curvature restrictions for flow in open-channel bends. *Journal of Geophysical Research* **115**: F04011. doi:10.1029/2009JF001301.

Braudrick CA, Dietrich WE, Leverich GT, Sklar LS. 2009. Experimental evidence for the conditions necessary to sustain meandering in coarse-bedded rivers. *Proceedings of the National Academy of Sciences of the United States of America* **106**: 16936–16941. doi:10.1073/pnas.0909417106.

Camporeale C, Perona P, Poporato A, Ridolfi L. 2007. Hierachy of models for meandering rivers and related morphodynamic processes. *Reviews of Geophysics* **45**: RG1001. doi:10.1029/2005RG000185.

Chen D, Tang C. 2012. Evaluating secondary flows in the evolution of sine-generated meanders. *Geomorphology* **163–164**: 37–44.

Constantine CR, Dunne T, Hanson GJ. 2009. Examining the physical meaning of the bank erosion coefficient used in meander migration modeling. *Geomorphology* **106**: 242–252.

Constantinescu G, Kashyap S, Tokyay T, Rennie CD, Townsend RD. 2013. Hydrodynamic processes and sediment erosion mechanisms in an open channel bend of strong curvature with deformed bathymetry. *Journal of Geophysical Research: Earth Surface* **118**: 1–17. doi:10.1002/jgrf/20042.

Crosato A. 1987. Simulation model of meandering processes of rivers. In Euromech 215: Mechanics of Sediment Transport in Fluvial and Marine Environments. University of Genoa: Genoa, Italy.

Crosato A, Saleh MS. 2011. Numerical study on the effects of floodplain vegetation on river planform style. *Earth Surface Processes and Landforms* **36**: 711–720. doi:10.1002/esp.2088.

Edmonds DA, Slingerland RL. 2008. Stability of delta distributary networks and their bifurcations. *Water Resources Research* **44**: W09426. doi:10.1029/2008WR006992.

Engel FL, Rhoads BL. 2012. Interaction among mean flow, turbulence, bed morphology, bank failures and channel planform in an evolving compound meander loop. *Geomorphology* **163–164**: 70–83. doi:10.1016/j.geomorph.2011.1005.1026.

Frascati A, Lanzoni S. 2013. A mathematical model for meandering rivers with varying width. *Journal of Geophysical Research: Earth Surface* **118**: 1641–1657. doi:10.1002/jgrf.20084.

Güneralp I, Rhoads BL. 2009. Empirical analysis of the planform curvature-migration relation of meandering rivers. *Water Resources Research* **45**: W09424. doi:10.1029/2008WR007533.

Güneralp I, Rhoads BL. 2010. Spatial autoregressive structure of meander evolution revisited. *Geomorphology* **120**: 91–106. doi:10.1016/j.geomorph.2010.02.010.

Güneralp I, Rhoads BL. 2011. Influence of floodplain erosional heterogenerity of planform complexity of meandering rivers. *Geophysical Research Letters* **38**: L14401. doi:10.1029/2011GL048134.

Güneralp I, Marston RA. 2012. Process-form linkages in meander morphodynamics: bridging theoretical modeling and real world complexity. *Progress in Physical Geography* **36**: 718–746. doi:10.1177/0309133312451899.

Howard AD. 1992. Modeling channel migration and floodplain sedimentation in meandering streams. In Lowland Floodplain Rivers: Geomorphological Perspectives, Carling P, Petts GE (eds). John Wiley and Sons: Chichester; 1–41.

Howard AD. 1996. Modelling channel evolution and floodplain morphology. In Floodplain Processes, Anderson MG, Walling DE, Bates PD (eds). John Wiley & Sons: Chichester; 15–62.

Howard AD, Knutson TR. 1984. Sufficient conditions for river meandering: a simulation approach. *Water Resources Research* **20**(11): 1659–1667.

Ikeda S, Parker G, Sawai K. 1981. Bend theory of river meanders. I. Linear development. *Journal of Fluid Mechanics* **112**: 363–377.

Johannesson J, Parker G. 1989. Linear theory of river meanders. In River Meandering, Ikeda S, Parker G (eds). Water Resources Monograph 12, American Geophysical Union: Washington, D.C.; 181–214.

Keylock CJ, Hardy RJ, Parsons DR, Ferguson RI, Lane SN, Richards KS. 2005. The theoretical foundations and potential for large-eddy simulation (LES) in fluvial geomorphic and sedimentological research. *Earth-Science Reviews* **71**: 271–304.

Larsen EW, Fremier AlK, Girvetz EH. 2006. Modeling the effects of variable dannual flow on river channel migration patterns, Sacramento rover, California, USA. *Journal of the America Water Resources Association* **42**: 1063–1075.

Leopold LB, Wolman MG. 1960. River Meanders. *Bulletin of Geological Society of America* **71**: 769–794.

Luchi R, Zolezzi G, Tubino M. 2011. Bend theory of river meanders with spatial width variations. *Journal of Fluid Mechanics* **681**: 311–339. doi:10.1017/jfm.2011.200.

Luchi R, Bolla Pittaluga R, Seminara G. 2012. Spatial width oscillations in meandering rivers at equilibrium. *Water Resources Research* **48**: W05551. doi:10.1029/2011WR011117.

Luppi L, Rinaldi M, Teruggi LB, Darby SE, Nardi L. 2008. Monitoring and numberical modeling of river bank erosion processes: a case study along the Cecina River (central Italy). *Earth Surface Processes and Landforms* **34**: 530–546. doi:10.1002/esp.1754.

Motta D, Abad JD, Langendoen EJ, Garcia MH. 2012. A simplified 2D model for meander migration with physically-based bank evolution. *Geomorphology* **163–164**: 10–25. doi:10.1016/j.geomorph.2011.1006.1036.

Nanson GC. 1980. Point bar and floodplain formation of the meandering Beatton River, northeastern British Columbia, Canada. *Sedimentology* **27**: 3–29. doi:10.1111/j.1365-3091.1980.tb01155.x.

Nanson GC, Hickin EJ. 1983. Channel migration and incision on the Beatton River. *Journal of Hydraulic Engineering* **109**(3): 327–337.

Ottevanger W, Blanckaert K, Uijttewaal WSJ. 2012. Processes governing the flow redistribution in sharp river bends. *Geomorphology* **163–164**: 45–55. doi:10.1016/j.geomorph.2011.1004.1049.

Page KJ, Nanson GC, Frazier PS. 2003. Floodplain formation and sediment stratigraphy resulting from oblique accretion on the Murrumbidgee River, Australia. *Journal of Sedimentary Research* **73**: 5–14.

Parker G, Shimizu Y, Wilderson GV, Eke EC, Abad JD, Lauer JW, Paola C, Dietrich WE, Voller VR. 2011. A new framework for modeling the migration of meandering rivers. *Earth Surface Processes and Landforms* **36**: 70–86.

Perucca E, Camporeale C, Ridolfi L. 2007. Significance of the riparian vegetation dynamics on meandering river mophodynamics. *Water Resources Research* **43**: W03430. doi:10.1029/2006WR005234.

Pizzuto JE, Meckelnburg TS. 1989. Evaluation of a linear bank erosion equation. *Water Resources Research* **25**(5): 1005–1013.

Richards K. 1982. Rivers: Form and Process in Alluvial Channels. Cambridge University Press: Cambridge.

Roelvink JA, van Banning GKFM. 1994. Design and development of DELFT3D and application to coastal morphodynamics. In Hydroinformatics '94, Verwey A, Minns AW, Babovic V, Maksimovic C (eds). A. A. Balkema: Brookfield, Vt; 451–456.

van Sabben A. 2010. Sharp Bend Flow: Comparison of Delft3d-FLOW with LES and Measurements for Sharp Bends. MSc thesis, Delft University of Technology, Delft, Netherlands.

Seminara G. 2006. Meanders. *Journal of Fluid Mechanics* **554**: 271–297.

Seminara G, Tubino M. 1989. Alternate bars and meandering: free, forced and mixed interactions. In River Meandering, Ikeda S, Parker G (eds). American Geophysical Union: Washington, DC; 153–180.

Seminara G, Pittaluga MB. 2012. Reductionist versus holistic approaches to the study of river meandering: an ideal dialog. *Geomorphology* **163–164**: 110–117.

Seminara G, Zolezzi G, Tubino M, Zardi D. 2001. Downstream and upstream influence in river meandering. Part 2. Planimetric development. *Journal of Fluid Mechanics* **438**: 213–230.

Sun T, Jøssang T, Meakin P, Schwarz K. 1996. A simulation model for meandering rivers. *Water Resources Research* **32**: 2937–2954.

Tubino M, Seminara G. 1990. Free-forced interactions in developing meanders and suppression of free bars. *Journal of Fluid Mechanics* **214**: 131–159.

US Army Corps of Engineers (USACE). 2010. HEC-RAS river analysis system, User's Manual, CPD-68. http://www.hec.usace.army.mil/software/hec-ras/documentation/HEC-RAS_4.1_Users_Manual.pdf. [Last accessed 9 May 2014]

Williams GP. 1978. Bank-full discharge of rivers. *Water Resources Research* **14**: 1141–1154.

Xu D, Bai Y, Ma J, Tan Y. 2011. Numerical investigation of long-term planform dynamics and stability of river meandering on fluvial floodplains. *Geomorphology* **132**: 195–207.

Zolezzi G, Seminara G. 2001. Downstream and upstream influence in river meandering. Part 1. General theory and application to overdeepening. *Journal of Fluid Mechanics* **438**: 183–211.